J Solid State Electrochem (2011) 15:2253–2264
DOI 10.1007/s10008-010-1240-4

ORIGINAL PAPER

Magnesium ion-conducting gel polymer electrolytes dispersed with fumed silica for rechargeable magnesium battery application

G. P. Pandey · R. C. Agrawal · S. A. Hashmi

Received: 18 May 2010 / Revised: 7 November 2010 / Accepted: 9 November 2010 / Published online: 25 November 2010

Abstract Effect of fumed silica dispersion on poly(vinylidene fluoride-co-hexafluoropropylene)-based magnesium ion-conducting gel polymer electrolyte has been studied using various physical and electrochemical techniques. The composite gel electrolytes are free-standing and flexible films with enough mechanical strength. The optimized composition with 3 wt.% filler offers a maximum ionic conductivity of ~1.1×10^{-2} Scm^{-1} at ~25 °C with good thermal and electrochemical stabilities. The Mg^{2+} ion conduction in the gel nanocomposite film is confirmed from the cyclic voltammetry, impedance spectroscopy, and transport number measurements. The space-charge layers formed between filler particles and gel electrolyte are responsible for the enhancement in ionic conductivity. The applicability of the gel nanocomposite to a rechargeable battery is examined by fabricating a prototype cell consisting of Mg [or Mg-multiwalled carbon nanotube (MWCNT) composite] and MoO_3 as negative and positive electrodes, respectively. The discharge capacity and the rechargeability of the cell have been improved when Mg metal is substituted by Mg-MWCNT composite. The discharge capacity of the optimized cell has found to be ~175 $mAhg^{-1}$ of MoO_3 for an initial ten charge–discharge cycles.

Keywords Gel polymer electrolyte · Magnesium ion conductor · Nanocomposite · AC impedance spectroscopy · Cyclic voltammetry

G. P. Pandey · S. A. Hashmi (✉)
Department of Physics and Astrophysics, University of Delhi,
Delhi 110 007, India
e-mail: sahashmi@physics.du.ac.in

G. P. Pandey · R. C. Agrawal
School of Studies in Physics,
Pandit Ravishankar Shukla University,
Raipur 492010 Chhattisgarh, India

Introduction

Polymer-based electrolytes are materials of technological interest due to their use in various electrochemical applications [1–4]. Various combinations of salts, plasticizers, and polymers have been investigated with a particular attention to the systems for lithium battery application [1–6]. A family of electrolytes, specifically referred as gel polymer electrolytes, has recently found global interest due to their specific electrochemical properties, which make them suitable for various technological applications including rechargeable batteries, supercapacitors, fuel cells, etc. [1–6]. These materials are formed by immobilizing the salt solutions (for example, $LiClO_4$ in propylene carbonate) in the host polymers such as poly (vinylidene fluoride-co-hexafluoropropylene) (PVdF-HFP), poly(methyl methaacrylate) (PMMA), polyacrylonitrile (PAN), etc. [1–4, 7–10]. The gel electrolytes have some important advantages over liquid electrolytes in that the risk of leakage is reduced, and electrode-electrolyte interfacial contact can be maintained during volumetric changes associated with charge and discharge cycling of the batteries. However, the main drawbacks associated with these materials are their poor dimensional stability, reduction in the electrical conductivity with time, interfacial instability towards electrode materials, which are deleterious in terms of poor reliability and safety of the devices.

In order to improve the mechanical, electrical, and electrochemical properties of the gel polymer electrolytes and their integrity during operation and storage, various approaches are adopted. The dispersion of micro- or nano-sized ceramic fillers, e.g., Al_2O_3, SiO_2, MgO, TiO_2, etc. is one of the most reported approaches to improve the dimensional as well as the electrical and electrochemical properties of polymer/gel electrolytes [2, 11–15]. Such

composite gel electrolytes preserve a porous structure due to dispersion of fillers, which lead to maximize the adsorption of liquid electrolyte and to reduce the risk of leakage [12–15].

Presently, global attention is devoted to develop advanced battery technologies based on lithium, though rechargeable lithium metal batteries with high specific capacities are still commercially unavailable. To date, the rechargeable lithium-ion battery has been one of the best choices in view of its specific capacity and cycle stability [16]. Nevertheless, lithium-ion batteries are relatively expensive and suffer from some safety limitations. Recently, the magnesium-based rechargeable battery system has attracted attention due to its performance capabilities that are close to those of lithium-based alternatives [17–19]. Magnesium is an attractive anode material for high energy density batteries as it has high charge density (low electrochemical equivalence ~12.15 g eq^{-1}) and considerably negative electrode potential (−2.356 V vs. NHE). Also, the material is cost effective due to natural abundance and safer than lithium that is presently used in practical high energy density batteries. Recently, Aurbach and coworkers have developed a prototype high-capacity rechargeable magnesium battery using electrolyte solutions based on Mg organohaloaluminate salts [17]. They have shown that Chevrel phases Mo_6S_8 can insert Mg ions reversibly and can be used as practical cathode materials for rechargeable Mg batteries [20, 21]. Despite these studies, however, the rechargeable Mg batteries are still in the developing stage mainly due to the poor reversibility of the Mg-negative electrode and lack of suitable non-aqueous electrolytes. It has been reported that the poor behavior of Mg electrode is caused by passivation phenomena and surface film formation processes at the electrode-electrolyte interfaces [18, 22]. Surface films effectively block the electrodes, as the mobility of the Mg^{2+} ions in the passivating films is extremely low [23]. From the electrolyte point of view, gel polymer electrolytes may be useful to overcome different problems and solid-state rechargeable Mg batteries can be realized using the solid-state Mg^{2+} ion-conducting gel polymer electrolytes [19, 24].

In the present study, the effect of dispersion of fumed silica in a PVdF-HFP-based Mg^{2+} ion-conducting gel polymer electrolyte is investigated by means of various physical techniques, namely, X-ray diffraction, thermal analysis, infrared spectroscopy, complex impedance analysis, cyclic voltammetry, and transport number measurements. A prototype Mg cell is fabricated using the optimized composite gel polymer electrolyte. The charge and discharge characteristics of the cell have been examined to evaluate the applicability of the composite gel electrolyte to solid-state rechargeable Mg batteries.

Experimental

Materials

The copolymer, PVdF-HFP (~Mw 400,000, pellets), ethylene carbonate (EC), propylene carbonate (PC), magnesium perchlorate [$Mg(ClO_4)_2$], and fumed silica (particle size ~7 nm) were obtained from Sigma-Aldrich. The intermediate solvent tetrahydrofuran (THF) was purchased from Merck, India. Magnesium salt and fumed silica were vacuum dried at 100 °C before use. A solution cast method was used to prepare composite gel polymer electrolyte films. In this process, the liquid electrolyte was first prepared by dissolving 1.0 M $Mg(ClO_4)_2$ in a mixture of EC and PC (1:1 volume/volume). The host polymer PVdF-HFP was separately dissolved in THF by stirring it magnetically at ~50 °C and its different amount was mixed in liquid electrolyte. To prepare composite gel polymer electrolyte, fumed silica in different weight ratios (from 0 to 25 wt.% with respect to the polymer weight) were dispersed. In the composite gel polymer electrolyte, the ratio of polymer with respect to the liquid electrolyte was maintained to 1:4. The mixtures were then stirred thoroughly for ~10 h and the proper filler dispersion was ensured by keeping the mixture in an ultrasonic bath for about half an hour. Finally the mixtures were poured in glass Petri dishes and allowed to evaporate THF to obtain solid-like free-standing composite gel films of thickness ~300–400 μm.

Circular discs (area=1.3 cm^2) of magnesium electrodes were obtained by palletising the magnesium powder (Aldrich). These discs were polished with successive grades of emery paper to a smooth finish then washed thoroughly in acetone and dried. The cathode sheets were prepared using molybdenum oxide (MoO_3) (Aldrich). A mixture of MoO_3 (65 wt.%), graphite powder (25 wt.%), and 10 wt.% of the gel electrolyte as the binder was thoroughly mixed in a mortar and spread on flexible graphite sheets (15× 15 mm). The cathode sheets were heated at ~100 °C before cell fabrication. Mg-multiwalled carbon nanotube (MWCNT) composite anode was prepared by palletising the mixture of magnesium powder and MWCNT (Aldrich) in the ratio 4:1. A Mg or Mg-MWCNT|gel polymer electrolyte|MoO_3 cell was assembled by sandwiching the respective electrodes and the gel electrolyte film in a specially designed sealed container. Several cells were fabricated to ensure reproducibility of their various characteristics.

Instrumentation

The morphological studies of the gel polymer films were carried out using Scanning Electron Microscope (JEOL,

JSM 5600). The SEM micrographs were taken at low vacuum after sputtering the samples with gold to prepare a conductive surface. The X-ray diffraction (XRD) patterns of the gel polymer electrolyte films were recorded using Philips X-ray diffractometer at Cu-Kα radiation in the Bragg angle (2θ) range from 10° to 60°. The FTIR spectra of the thin composite gel polymer films were recorded with the help of Perkin-Elmer FTIR Spectrophotometer over a wavenumber range from 400 to 4,000 cm^{-1} at ambient temperature. The thermal stability of composite gels was tested by thermo-gravimetric analysis (TGA) and differential scanning calorimetry (DSC). TGA was carried out for the temperature range from room temperature to 475 °C under dynamic dry nitrogen atmosphere with a heating rate of 10 °Cmin^{-1} using Perkin-Elmer TGA system (TGA7). DSC was performed from −85 to 100 °C at a heating rate of 10 °Cmin^{-1} in the static nitrogen atmosphere with the help of DSC system of TA Instruments (Model: Q100).

The ionic conductivity of the gel films was evaluated by AC impedance spectroscopic technique over the frequency range from 1 Hz to 100 kHz using LCR Hi-Tester (Model: 3522-50, HIOKI, Japan). The signal level was kept at 10 mV. The ionic conductivity measurements were carried out by sandwiching the gel polymer films between two stainless steel (SS) electrodes over the temperature range from 25 to 80 °C. The area of SS-foils was 1.3 cm^2. A comparative cyclic voltammetric studies were carried out on the symmetric cells, sandwiching the composite gel polymer films between SS and Mg electrodes at a scan rate of 5 mVs^{-1} using an Electrochemical Analyzer (Model: CHI 608 C, CH Instruments, USA). The electrochemical stability of the gel polymer films was evaluated by means of linear sweep voltammetry using SS as the working electrode and Mg disc as combined counter and the reference electrodes. Total ionic transport number (t_{ion}) was evaluated by the polarization technique [25]. In this technique, the cell SS|gel polymer film|SS was polarized by applying a step potential of 1.0 V and the resulting potentiostatic current was monitored as a function of time. The stainless steel (SS) acted as blocking electrodes for the above cell. The "t_{ion}" was evaluated using the formula:

$$t_{ion} = \frac{i_T - i_e}{i_T} \quad (1)$$

where i_T and i_e are total and residual current respectively. The Mg^{2+} ions transport number (t_+) of the composite gel electrolytes was evaluated using the combination of AC impedance spectroscopy and DC polarization technique proposed by Evans et al. [26]. In this technique, the cells Mg|gel polymer films|Mg were polarized potentiostatically applying a voltage, ΔV=0.3 V for 3–4 h and subsequently initial and final currents were recorded. The cells were subjected to AC impedance measurements also prior to and after the polarization, as a part of the technique. The values of electrode-electrolyte contact resistances were obtained from the impedance plots. The t_+ values were obtained using the expression:

$$t_+ = \frac{I_s(\Delta V - R_0 I_0)}{I_0(\Delta V - R_s I_s)} \quad (2)$$

where I_0 and I_s are the initial and final currents. R_0 and R_s are cell resistances, before and after the polarization, respectively. The performances of Mg cell was investigated by a charge–discharge cycling test at room temperature (~25 °C) using Arbin instrument (model: BT 2000, USA) under different constant current conditions. The cut-off charging and discharging voltages were kept at 2.7 and 0.8 V, respectively.

Results and discussion

Structural properties

The morphology of the undispersed gel polymer electrolyte and composite gel polymer electrolyte film (with 10 wt.% fumed silica) has been examined by SEM, and the images are shown in Fig. 1. The undispersed gel polymer electrolyte film is observed to have uniform small pores at microscopic level (Fig. 1a). In the composite gel polymer electrolyte dispersed with fumed silica, slightly larger in size and uniformly distributed pores are observed (Fig. 1b). The uniformly dispersed pores in the polymer microstructure lead to the retention of liquid electrolyte and formation of their better connectivity through the polymer, giving rise to have possibility of high ionic conductivity.

XRD patterns of the PVdF-HFP (pure), undispersed polymer gel electrolyte and composite gel polymer electrolytes are shown in Fig. 2. The pattern of pure PVdF-HFP shows the typical characteristic of a semi-crystalline microstructure, i.e., the coexistence of mixed crystalline and amorphous nature of the material with predominant peaks at 2θ=14.6°, 17°, 20°, 26.6°, and 38°. The diffractogram of filler free gel polymer electrolyte shows a broadened peak between 10° and 30°. The PVdF-HFP peak at ~26.6° is masked in the broad peak and the intense peak at ~38° disappears (Fig. 2b). These changes reveal that the gel polymer electrolyte is predominantly amorphous and its crystallinity is depressed due to the immobilization of liquid electrolyte in PVdF-HFP. This indicates that the liquid electrolyte solution most likely blends with the PVdF-HFP at molecular level and functions as a plasticizer for the polymer. The diffractogram of composite gel polymer electrolyte dispersed with fumed silica shows the characteristic peaks of silica, observed at

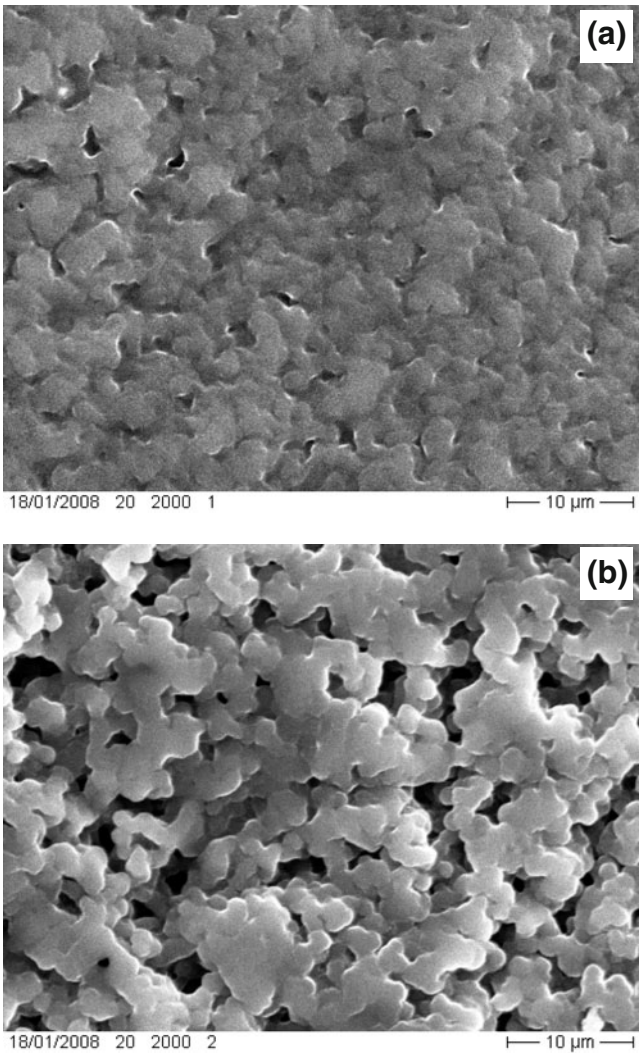

Fig. 1 SEM images of gel polymer electrolyte films containing fumed silica of: **a** 0 wt.% and **b** 10 wt.%

25.5° along with some PVdF-HFP peaks. These observations confirm the composite nature of the gel films.

FTIR spectroscopic investigation have been carried out to study the ion–polymer interaction and possible conformational changes in the host polymer due to the Mg salt containing liquid electrolyte entrapment and dispersion of fumed silica, Fig. 3 shows the comparative FTIR spectra of the host polymer PVdF-HFP and gel polymer electrolyte films dispersed with different amount of fumed silica (from 0 to 20 wt.%). Following distinctive features have been observed from these spectral responses:

1. The conformational changes in the semi-crystalline host polymer PVdF-HFP due to the addition of liquid electrolyte have been monitored. The Peaks at 528, 762, and 976 cm^{-1} are due to a non-polar *trans-gauche-trans-gauche*' conformation (i.e., α-phase) of the semi-crystalline PVdF-HFP [27–29]. The peak at 484 cm^{-1} is due to an intermediate polar TTTGTTTG' conformation (γ-phase), occurring when the polymer is moderately stressed [30]. Other bands are very weak and/or overlapped with the band associated with the EC–PC or Mg salt. It may be noted that the band at 762 cm^{-1} (assigned to α-phase) disappears due to the addition of liquid electrolyte. Furthermore, the bands at 839 and 879 cm^{-1}, assigned to amorphous phase, appear as a symmetrical peak. Both the bands shifted slightly and become sufficiently broad, appearing as the sum of two peaks, as shown in Fig. 3 (inset). These observations indicate the substantial conformational changes in the crystalline texture of the host polymer PVdF-HFP due to the interaction with liquid electrolyte. The disappearance of some bands associated with crystalline α-phase and appearance of the bands of amorphous phase of the polymer indicate the reduction of crystallinity and dominance of the amorphous phase in the composite gel polymer electrolyte.
2. The stretching vibration mode (ν_4) of ClO_4^- anion observed in the range of 650–600 cm^{-1} has been probed to get the information associated with the degree of salt dissociation in the composite gel polymer electrolyte. The expanded portion of the spectra in the range 650–600 cm^{-1} is shown in the Fig. 4a. The peaks

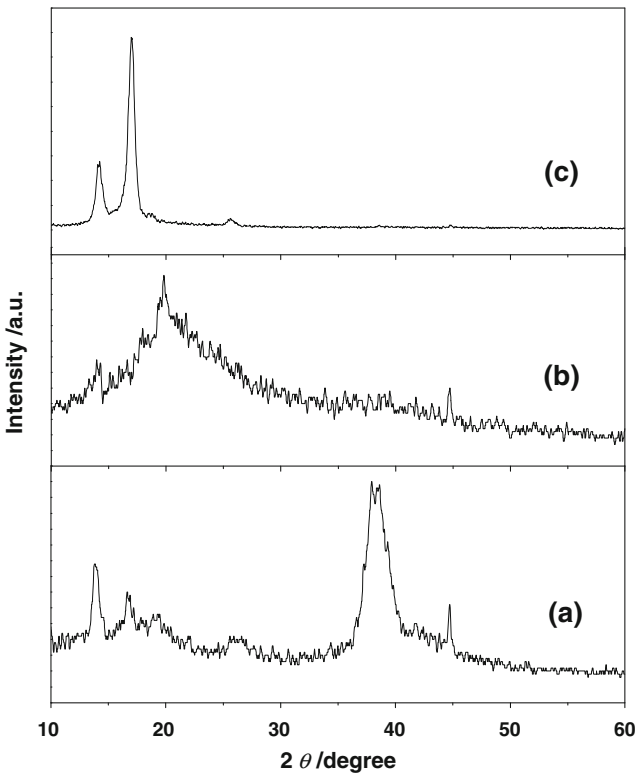

Fig. 2 XRD patterns of *a* pure PVdF-HFP, *b* EC–PC-$Mg(ClO_4)_2$+ PVdF-HFP gel polymer electrolyte and its composite film dispersed with *c* 10 wt.% of SiO_2 nanoparticles

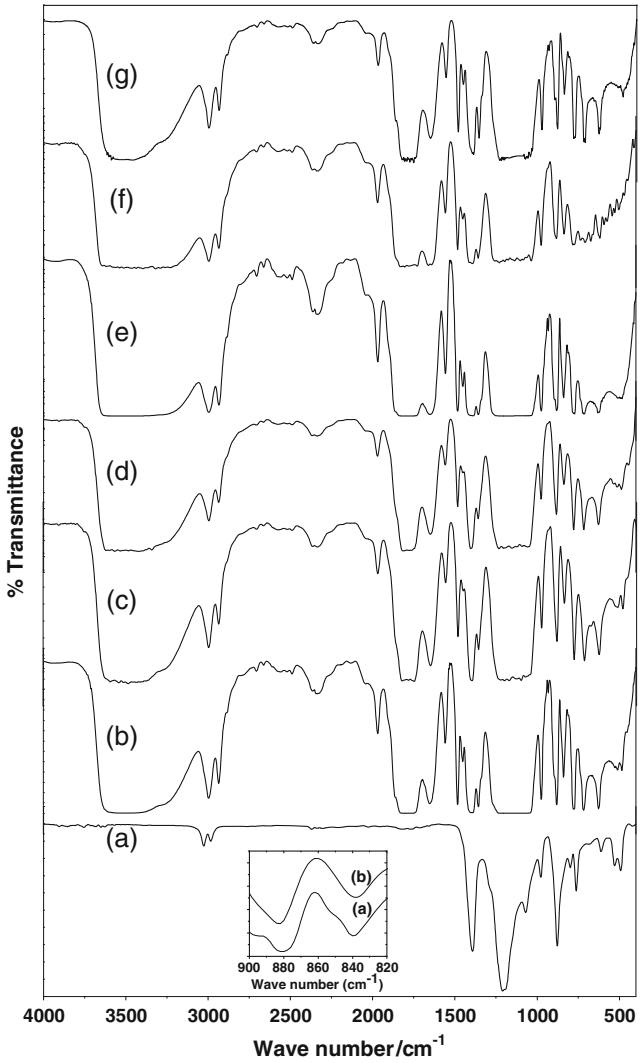

Fig. 3 FTIR spectra of *a* PVdF-HFP (pure) film and gel polymer electrolyte films containing fumed silica of *b* 0 wt.%, *c* 5 wt.%, *d* 7 wt.%, *e* 10 wt.%, *f* 15 wt.%, and *g* 20 wt.%. Expanded representation of the band of 839 and 879 cm^{-1} is shown in the *inset*

at ~628 and ~623 cm^{-1} are attributed to the ion-paired and the free anions $(ClO_4)^-$, respectively [31]. In the undispersed gel polymer electrolyte, the peak ~626 cm^{-1} appeared as the sum of two nearby peaks associated with the free and paired $(ClO_4)^-$ ions. The dispersion of fumed silica in the gel polymer electrolyte influences this band, the peak becomes broader and two peaks appear well separated. This indicates the filler–anion interaction in the composite gel polymer electrolytes. The dispersion of fumed silica in the gel polymer electrolyte affects the O–H stretching bands. These bands in the region 3,660–3,230 cm^{-1} get broadened, creating asymmetric wings toward lower frequency, as shown in the expanded portion of Fig. 4b. This indicates that hydroxyl groups adsorbed with fumed silica powder are involved in band interactions [32]. It is also likely

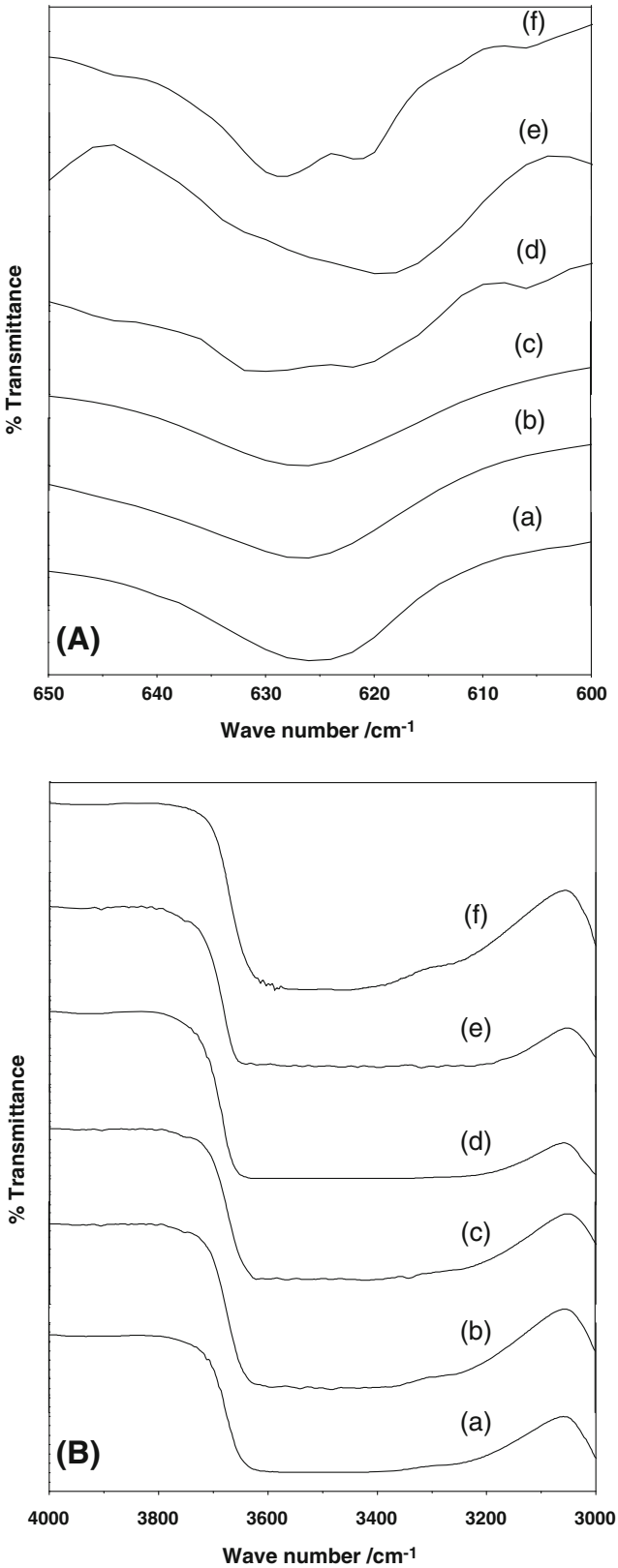

Fig. 4 Expanded representation of FTIR spectra of gel electrolyte nanocomposite films containing fumed silica of *a* 0 wt.%, *b* 5 wt.%, *c* 7 wt.%, *d* 10 wt.%, *e* 15 wt.%, and *f* 20 wt.% in **a** 600–650 cm^{-1} and **b** 3,000–4,000 cm^{-1} spectral regions

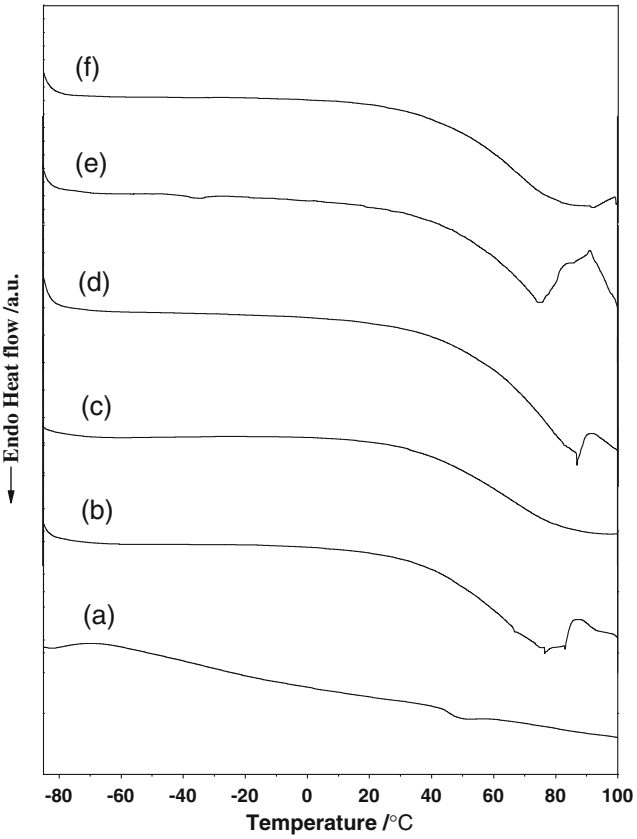

Fig. 5 DSC traces of *a* PVdF-HFP (pure) film and gel polymer electrolyte films containing *b* 0 wt.%, *c* 3 wt.%, *d* 5 wt.%, *e* 10 wt.%, and *f* 20 wt.% of fumed silica

that the surface hydroxyl groups on different fumed silica particles could be hydrogen bonded to one another [33]. These significant changes clearly indicate the substantial modifications in the lattice environment due to dispersion of fumed silica, which in turn affect the ion conduction in the composite gel polymer electrolytes significantly.

Thermal properties

Thermal studies have been carried out to find out a temperature stability range in which the gel electrolyte can be used safely in the electrochemical applications. For this purpose, DSC and TGA studies have been performed. Figure 5 shows the comparative DSC curves of pure PVdF-HFP film and the fumed silica containing composite gel polymer electrolytes. The glass transition temperature (T_g) has been observed at −65 °C for pure PVdF-HFP film (Fig. 5a). After the gel formation due to the addition of liquid electrolyte in host polymer, T_g value generally decreases, possibly below −90 °C in the present case, which is not observable due to the limitation of the equipment used. A peak corresponding to melting of the crystalline phase of host polymer PVdF-HFP has been observed ~90 °C and peak position is almost unaffected due to fumed silica dispersion. Furthermore, the composite gel polymer electrolytes remains stable in the same gel phase over a wide temperature range from −70 to 80 °C, which is substantial for their potential applications in the devices like batteries, etc.

Typical comparative TGA curves of pure PVdF-HFP, undispersed gel polymer electrolyte and composite gel polymer electrolyte (with 10 wt.% fumed silica) are shown in Fig. 6. The host polymer PVdF-HFP exhibit high thermal stability as almost no weight loss has been observed upto ~400 °C. A marginal weight loss (~5 wt.%) has been observed up to ~90 °C for both the undispersed and composite gel polymer electrolytes, which may be due to the surface adsorbed moisture. Thereafter, a substantial weight loss has started due to the evaporation of the solvents EC and PC.

Electrochemical characterization

Ionic conductivity

The composition of PVdF-HFP/EC/PC+1.0 M $Mg(ClO_4)_2$-based gel polymer electrolyte (without fillers) was optimized to get highly conducting and dimensionally stable material. For this purpose, the liquid electrolyte comprising of EC/PC (1:1 *v*/*v*)+1.0 M $Mg(ClO_4)_2$ was immobilized with different amount of PVdF-HFP. Figure 7 shows the variation of room temperature (~25 °C) ionic conductivity (σ) as a function of PVdF-HFP content in liquid electrolyte. The conductivity of liquid electrolyte has been observed to be $\sim 3 \times 10^{-3}$ S cm^{-1}. On addition of host polymer PVdF-

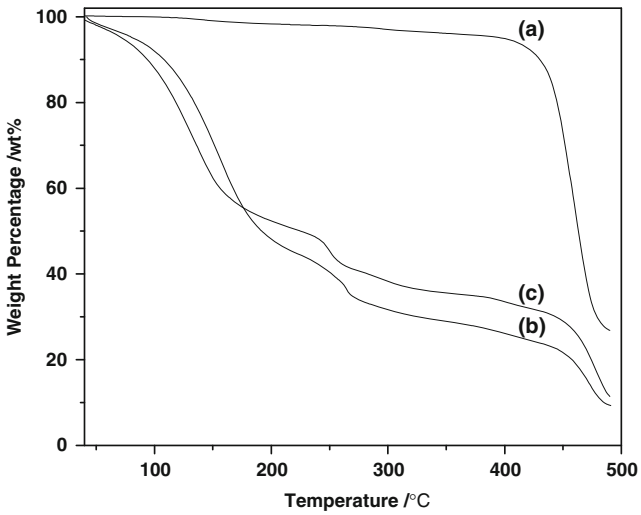

Fig. 6 TGA curves of *a* pure PVdF-HFP film and gel polymer electrolyte films containing *b* 0 wt.%, and *c* 10 wt.% of fumed silica

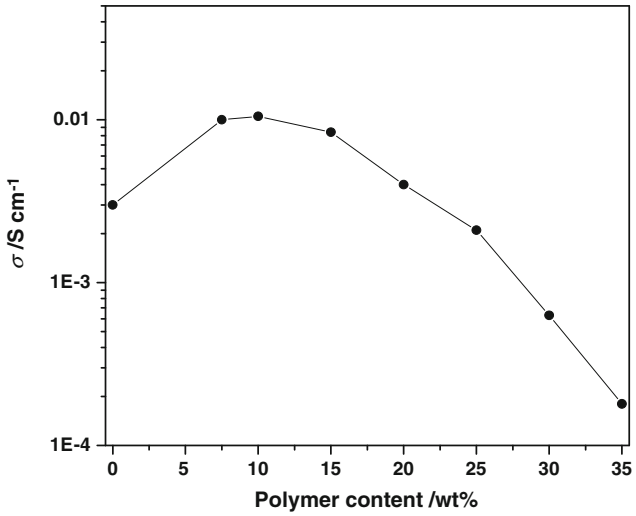

Fig. 7 Ionic conductivity of gel polymer electrolytes as a function of PVdF-HFP content

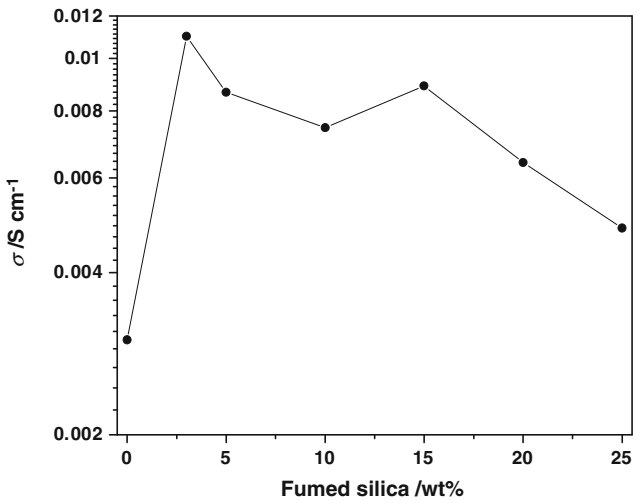

Fig. 8 Variation of room temperature ionic conductivity of gel polymer electrolyte nanocomposite films as function of fumed silica content

HFP, the conductivity initially increases (slightly), shows a maxima ($\sim 1\times10^{-2}$ Scm^{-1}) at ~10 wt.% of polymer and then it decreases on further addition of PVdF-HFP. Such conductivity variation in the gel polymer electrolytes has been reported earlier by a few workers [34, 35]. The distinct initial increase in the conductivity due to the addition of host polymer in the liquid electrolyte can be explained by the "breathing polymer chain model", suggested by Chandra and coworkers [35, 36]. According to this model, the polymer gel is considered to consist of dissociated ions, ion pairs, the solvent and polymer chains (folded or partially/fully unfolded chains). The polymer chains are assumed to breathe while they open or fold occupying different volume in the process. This leads to the localized pressure changes or fluctuations assisting either in breaking the ion pairs or unblocking of the viscosity controlled mobility, both resulting into a conductivity enhancement. It is interesting to note that the conductivity of the gel electrolyte with 20 wt.% of PVdF-HFP has been found to be almost same as that of the liquid electrolyte. Such composition is obtained in the form of free-standing film, dimensionally stable enough to handle. Therefore, this composition [EC/PC (1:1 *v*/*v*)+1.0 M $Mg(ClO_4)_2$+20 wt.% PVdF-HFP] has been chosen to make composite gel polymer electrolytes dispersing fumed silica powder.

The variation of room temperature ionic conductivity of composite gel polymer electrolytes with respect to the content of fumed silica particles is shown in Fig. 8. The addition of fumed silica particles results an initial increase in the conductivity of gel polymer electrolytes followed by two maxima at ~3 and ~15 wt.%. Such two maxima behavior has recently been reported by few workers for the gel polymer electrolyte composites and solvent-free composite polymer electrolytes [37–41]. The first conductivity maxima is possibly due to the dissociation of ion aggregates/undissociated salt into free ions with the addition of filler particles whereas the second conductivity maxima is related to the composite effect and explained on the basis of formation of a conducting interfacial space-charge double layer between the filler particles and polymer gel electrolytes [42–44]. The decrease in conductivity after the second conductivity maxima is generally related to the blocking effect of filler particles, which hinders the motion of mobile ions [45].

Figure 9 shows the temperature dependence of ionic conductivity of composite gel films. The "σ versus 1/*T*"

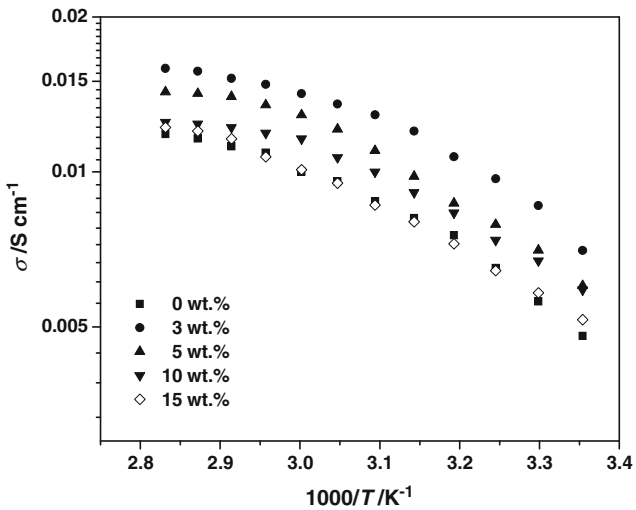

Fig. 9 Temperature dependence of ionic conductivity of gel polymer electrolyte films containing different amount of fumed silica

curves show the non-linear behavior, which follow the Vogel–Tammen–Fulcher equation expressed as:

$$\sigma = AT^{-1/2}\exp\left(\frac{-B}{T-T_0}\right) \quad (3)$$

where the parameter B has the dimension of energy and is related to the critical free volume for ion transport, A is a pre-exponential factor, i.e., the conductivity at infinitely high temperature and T_0 is equilibrium glass transition temperature close to the T_g values. These parameters have been evaluated by non-linear least square fitting of the data and listed in Table 1. From the temperature dependent ionic conductivity measurements, it may be noted that the optimized Mg^{2+} composite gel polymer electrolyte exhibits ionic conductivity of the order of $\sim 10^{-3}$ Scm^{-1} at 25 °C and $\sim 10^{-2}$ Scm^{-1} at 80 °C, showing promise for potential application in Mg batteries in a substantially wider temperature range.

Transport number

The total ionic transport number (t_{ion}) has been evaluated using polarization method, as described in the "Experimental". In this method, a typical cell: SS|gel polymer electrolyte|SS is polarizing through applying a voltage of 1.0 V across it and current has been monitored as a function of time. The value of t_{ion} is evaluated using Eq. (1) and found to be >0.99 for all the composite gel films. This shows that the overall conductivity of the pure gel electrolyte and gel composites is predominantly ionic. No electronic conductivity is expected in the gel like electrolytes where liquid electrolytes are entrapped in the almost inert network of polymer hosts and liquid-like charge transport takes place in such systems.

In order to evaluate the contribution of cations (and hence anions) to the overall conductivity, the cationic transport number (t_+) of Mg^{2+} ions in gel electrolyte films has been evaluated at room temperature using the combination of AC and DC techniques, as described in the "Experimental". A typical DC polarization "current versus time" plot for the cell Mg | composite gel | Mg is shown in Fig. 10. The AC impedance plots of the cell taken before and after polarization are also shown in Fig. 10 (inset). The values of the t_+, evaluated using Eq. 2 for the composite gel polymer electrolyte films, are listed in Table 2. A slight (but not very significant) increase in Mg^{2+} ion transport number has been observed due the dispersion of fumed silica. It may be noted that in the same range of silica dispersion, the ionic conductivity increases substantially, as described in the "Ionic conductivity". It is well established that the chemistry of filler particle surface, which form electrical space-charge double layer with gel electrolyte, plays an important role in the ion–surface interaction and have impact on ion conduction in composite electrolytes. As the filler in the present case (i.e., fumed silica) belongs to acidic oxides, it provides additional sites for anionic mobility in the gel electrolyte and filler interfaces. Hence, the substantial increase in conductivity is due to the combined effects of slight enhancement in Mg^{2+} transport number and

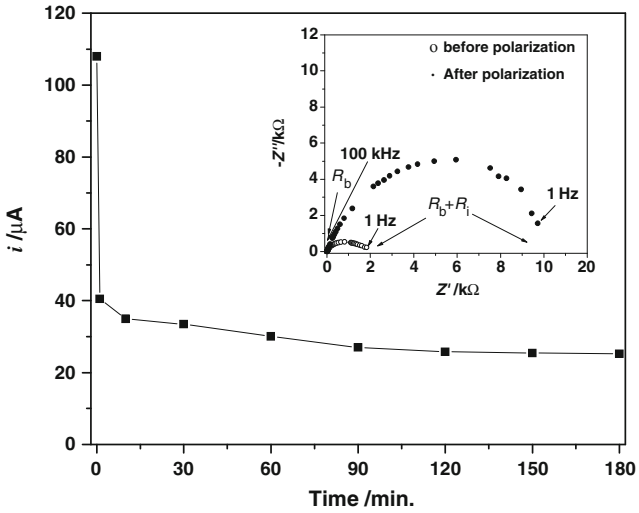

Fig. 10 DC polarization curve of a typical symmetric Mg|composite gel with 10 wt.% SiO_2|Mg cell, recorded at room temperature. AC complex impedance plots before and after polarization of cell is shown as *inset*

Table 1 A, B, and T_0 values for fumed silica dispersed gel polymer electrolytes obtained by non-linear least square fitting of conductivity data to VTF equation

Fumed silica content (wt.%)	Parameters		
	A ($Scm^{-1}K^{1/2}$)	B (eV)	T_0 (K)
0	2.51	0.053	179
3	1.21	0.022	181
5	1.33	0.026	178
10	1.69	0.028	180
15	2.12	0.032	186

VTF Vogel–Tammen–Fulcher

Table 2 Mg^{2+} ion transport number of gel polymer electrolyte containing different amount of fumed silica

Fumed silica (in wt.%)	Mg^{2+} ion transport number
0	0.22±0.02
3	0.28±0.02
5	0.26±0.02
10	0.28±0.02
15	0.30±0.02

dominant enhancement in anionic mobility in the space-charge regions.

Electrochemical properties

To confirm Mg^{2+} ion conduction in the composite gel polymer electrolytes, a complex impedance spectroscopy and cyclic voltammetric studies have been carried out on the following symmetrical cells:

Cell-A: SS|composite gel film|SS
Cell-B: Mg|composite gel film|Mg

In cell-A, the composite gel film was in contact with the SS (a blocking electrode) whereas foils of Mg was used as reversible electrodes in cell-B. Figure 11 shows the comparative complex impedance plots for cell-A and cell-B recorded at room temperature (~25 °C). The impedance response of cell-A shows the steep rising behavior of imaginary impedance at the lower frequency range, indicating the ion blocking nature of the SS electrodes. On the other hand, almost well-defined semicircular dispersion curve has been observed in the case of cell-B. The appearance of the well-defined semi-circle for the cell-B clearly suggests that the Mg metal attains equilibrium with the Mg^{2+} ions in the composite gel polymer electrolyte. Such behavior has also been reported for a Li|Li^+-gel electrolyte|Li cell [46]. These observations confirm Mg^{2+} ion conduction in the composite gel polymer electrolyte.

Figure 12 shows the cyclic voltammograms (CVs) for the cells containing gel electrolyte films with different amount of fumed silica sandwiched between two symmetrical Mg electrodes at a scan rate of 5 mVs^{-1}. The CV for the cell with symmetrical SS electrodes is also shown for comparison in Fig. 12 (inset). The cathodic and anodic current peaks are distinctly observed for the cells with Mg electrodes whereas no such features have been observed in the case of the cell with SS electrodes in the same potential range. This suggests the following reversible reaction:

$$Mg^{2+} + 2e^- \rightleftarrows Mg^0 \quad (4)$$

i.e., the cathodic deposition and anodic oxidation of Mg are facile at Mg/gel electrolyte interface. This confirms Mg^{2+} ion conduction in the composite gel polymer electrolyte films. Similar observation for the reversibility of Mg/Mg^{2+} couple in gel polymer has been reported by the other workers [24]. The changes in the anodic/cathodic current intensities are observed due to the different amount of fumed silica dispersion in gel composite system (Fig. 12). However, as the CV measurements have been performed in two-electrode configuration, it is difficult to explain these current variations distinctly. It may be noted that the cathodic/anodic peak potentials are separated by several volts because the experiments were carried out on the cells with two-electrode geometry without using reference electrode [47].

The electrochemical stability of the composite gel films has been tested using linear sweep voltammetry recorded on the cell: SS|composite gel polymer film|Mg. As observed from Fig. 13, the composite gel films are stable up to ~3.5 V vs. SS electrode. This value of working voltage range (i.e., electrochemical potential window) appears to be high enough to use the composite gel electrolyte films as solid-state-like separator/electrolyte in Mg batteries and supercapacitors.

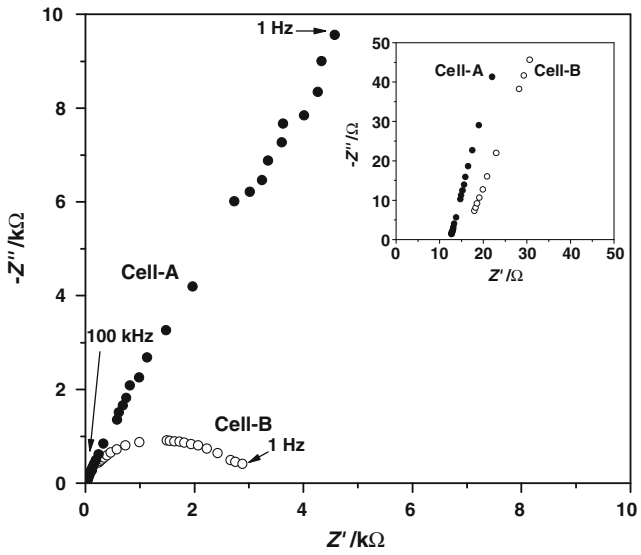

Fig. 11 Complex impedance plots for cell-A: SS|gel nanocomposite|SS and cell-B: Mg|gel nanocomposite|Mg at room temperature. High-frequency region is expanded and shown in inset

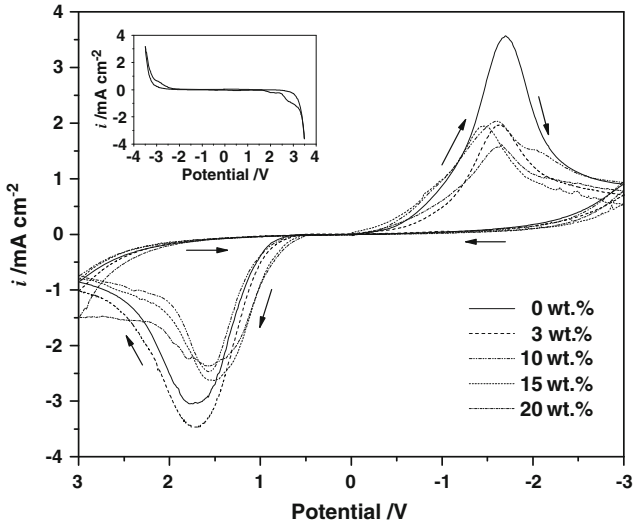

Fig. 12 Cyclic voltammograms of cell: Mg|gel nanocomposite|Mg with different amount of fumed silica, recorded at room temperature at the scan rate of 5 mVs^{-1}. Cyclic voltammogram of cell: SS|gel nanocomposite|SS is shown in *inset*

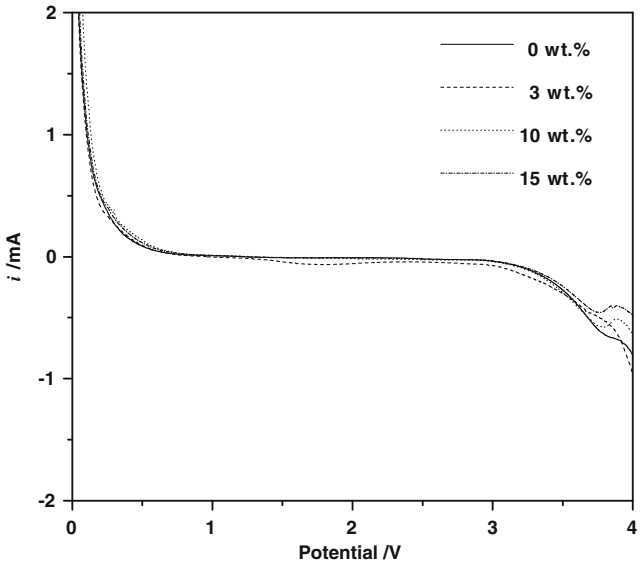

Fig. 13 Linear sweep voltammograms of SS|gel nanocomposite|Mg cells with different fumed silica content at the scan rate of 5 $mV s^{-1}$

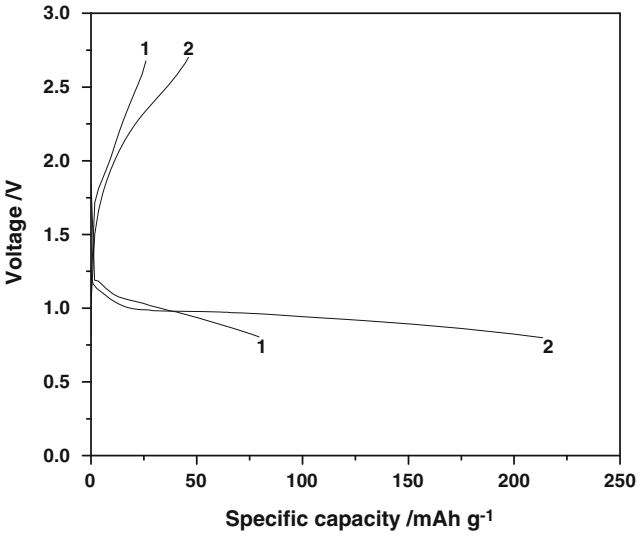

Fig. 14 Charge–discharge curves of the Mg|gel nanocomposite|MoO_3 cell at constant current of 0.2 $mA cm^{-2}$. *Numbers marked on the curves* represent the cycle numbers

Performance of Mg cells

In order to examine the applicability of the composite gel electrolyte to rechargeable magnesium battery systems, we fabricated prototype cells consisting of a MoO_3 cathode, Mg metal (or Mg-MWCNT composite) anode and optimized composite gel electrolyte film (with 3 wt.% SiO_2). The electrochemical insertion of divalent Mg^{2+} cations into orthorhombic MoO_3 has been reported in the literature [18, 48]. The open circuit voltage (OCV) of the Mg/MoO_3 has been observed to be around 1.85 V. The OCV has been found to be slightly reduced to ~1.65 V, when Mg-MWCNT composite anode was used instead of Mg anode. The cells were allowed to equilibrate under open circuit conditions for about 2 h before these were tested by charge–discharge studies. Figure 14 shows typical discharge and recharge curves of the Mg/MoO_3 cells using composite gel electrolyte under constant current condition (0.2 $mA cm^{-1}$). A potential plateau has been observed at ~1.0 V during the discharge for only first two to three cycles. The discharge capacity was about 200 mAh g $(MoO_3)^{-1}$ for the second cycle. However, the cell has low capacity (~50 $mAh g^{-1}$ of MoO_3) for recharging. This is mainly due to the electrochemical irreversibility of metallic Mg in nonaqueous media as reported earlier by other workers [22, 49]. When the Mg metal anode has substituted by Mg-MWCNT composite, the discharge capacity of the cell (Mg-MWCNT/MoO_3), at 0.1 $mA cm^{-1}$ constant current condition, has been found 225 mAh g $(MoO_3)^{-1}$ for first discharge cycle, as shown in Fig. 15. When charged by the same magnitude of charge, the cell voltage increased up to 2.7 V and charge capacity has been found about 75 mAh g $(MoO_3)^{-1}$. The cycle life data of Mg-MWCNT|composite gel electrolyte|MoO_3 cell is shown as inset of Fig. 15. An average discharge capacity of about 175 $mAh g^{-1}$ of MoO_3 is obtained during the initial ten charge/discharge cycles. Subsequently, the discharge capacity starts decreasing and cell voltage exceeded beyond the electrochemical potential window of the composite gel (~3.5 V) during charging. Therefore, further cycling of the cell could not be continued. The lower discharge capacity and poor rechargeability of the cell were mainly due to the high impedance at the interface between Mg metal and gel polymer

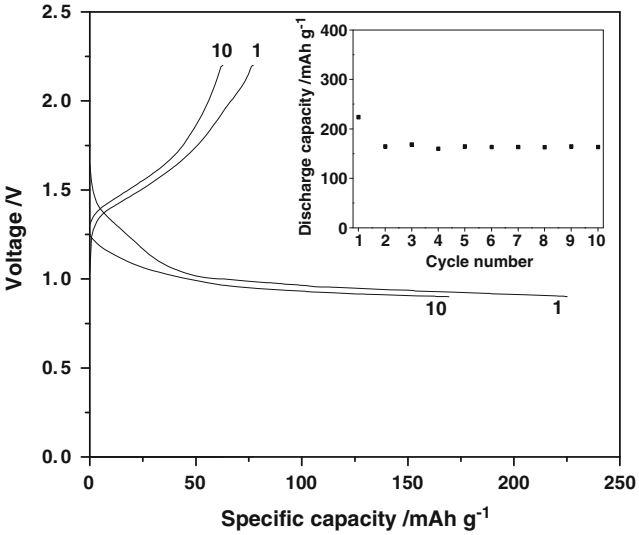

Fig. 15 Charge–discharge curves of the Mg-MWCNT|gel nanocomposite|MoO_3 cell at constant current of 0.1 $mA cm^{-2}$. *Numbers marked on the curves* represent the cycle numbers. Discharge capacity of the cell as a function of cycle number is shown in inset. Charge–discharge cycling was conducted between 0.8 and 2.7 V

electrolyte interface. Some improvement in the rechargeability (i.e., cyclic property) has been observed when Mg-MWCNT composite anode is used. Further investigation including a search of the suitable negative and positive electrode materials is in progress.

Conclusions

The nanocomposites of PVdF-HFP-based Mg^{2+} ion conducing gel polymer electrolyte dispersed with fumed silica powder have been synthesized and characterized using various experimental techniques. The dispersion of fumed silica in gel electrolytes has been found to be beneficial to improve their mechanical and electrochemical properties. On the basis of various physical and electrochemical studies, the following conclusions are drawn:

1. The gel electrolyte nanocomposites are obtained in the form of flexible and free-standing films with good dimensional stability.
2. Immobilization of liquid electrolyte and dispersion of fumed silica in gel polymer electrolyte lead to the substantial conformational changes in the crystalline texture of the host polymer PVdF-HFP and ion-filler-polymer interaction as confirmed from FTIR studies.
3. The ionic conductivity of gel nanocomposites increases significantly due to dispersion of fumed silica. The optimized composition of gel electrolyte offers high ionic conductivity of $\sim 1.1\times10^{-2}$ Scm^{-1} at room temperature with ~3 wt.% of silica.
4. The electrolytes show a wider electrochemical potential window and good thermal stability having single-phase behavior over a temperature range from −70 to 80 °C.
5. Studies based on AC impedance spectroscopy and cyclic voltammetry indicate the existence of an electrochemical equilibrium between Mg metal and Mg^{2+} ions and hence confirm Mg^{2+} ion conduction in the gel polymer electrolyte nanocomposite.
6. Prototype solid-state Mg (or Mg-MWCNT composite)|gel nanocomposite gel|MoO_3 cells have been assembled and characterized with charge–discharge tests for various cycles. Discharge capacity of ~175 $mAhg^{-1}$ of MoO_3 is obtained for the cell with Mg-MWCNT composite anode for more than 10 cycles. Efforts for further improvement in discharge capacity and cycle life of the Mg batteries are continued.

Acknowledgments Authors acknowledge the financial supports received from the Council of Scientific and Industrial Research (CSIR), New Delhi (Sanction No.: 03(1069)/06/EMR-II, 2006) and University of Delhi (under the Scheme 11-17 Research Fund). GPP is grateful to the Council of Scientific and Industrial Research (CSIR), New Delhi for the award of Research Associateship.

References

1. Song JY, Wang YY, Wan CC (1999) J Power Sources 77:183–197
2. Agrawal RC, Pandey GP (2008) J Phys D Appl Phys 41:223001–223018
3. Ciuffa F, Croce F, D'Epifanio A, Panero S, Scrosati B (2004) J Power Sources 127:53–57
4. Stephan AM (2006) Euro Polym J 42:21–42
5. Dias FB, Plomp L, Veldhuis JBJ (2000) J Power Sources 88:169–191
6. Schalkwijk WAV, Scrosati B (eds) (2002) Advances in Lithium-Ion Batteries. Kluwer/Plenum Publisher, New York
7. Kim HS, Periasamy P, Moon SI (2005) J Power Sources 141:293–297
8. Vondrak J, Reiter J, Velicka J, Klapste B, Sedlarıkova M, Dvorak J (2005) J Power Sources 146:436–440
9. Akashi H, Shibuya M, Orui K, Shibamoto G, Sekai K (2002) J Power Sources 112:577–582
10. Quartarone E, Tomasi C, Mustarelli P, Appetecchi GB, Croce F (1998) Electrochem Acta 43:1435–1439
11. Slane S, Salomon M (1995) J Power Sources 55:7–10
12. Tarascon JM, Gozdz AS, Schmutz CN, Shokoohi FK, Warren PC (1996) Solid State Ionics 86–88:49–54
13. Appetecchi GB, Romagnoli P, Scrosati B (2001) Electrochem Commun 3:281–284
14. Gentili V, Panero S, Reale P, Scrosati B (2007) J Power Sources 170:185–190
15. Pandey GP, Agrawal RC, Hashmi SA (2009) J Power Sources 190:563–572
16. Tarascon JM, Armand M (2001) Nature 414:359–367
17. Aurbach D, Lu Z, Schechter A, Gofer Y, Gizbar H, Turgeman R, Cohen Y, Moshkovich M, Levi E (2000) Nature 407:724–727
18. Novak P, Imhof R, Haas O (1999) Electrochim Acta 45:351–367
19. Pandey GP, Hashmi SA (2009) J Power Sources 187:627–634
20. Lancry E, Levi E, Gofer Y, Levi M, Salitra G, Aurbach D (2004) Chem Mater 16:2832–2838
21. Aurbach D, Suresh GS, Levi E, Mitelman A, Mizrahi O, Chusid O, Brunelli M (2007) Adv Mater 19:4260–4267
22. Morita M, Yoshimoto N, Yakushiji S, Ishikawa M (2001) Electrochem Solid State Lett 4:A177–A179
23. Miles MH, Park KH, Stilwell DE (1990) J Electrochem Soc 137:3393–3400
24. Kumar GG, Munichandraiah N (1999) Electrochim Acta 44:2663–2666
25. Hashmi SA, Chandra S (1995) J Mater Sci Eng B 34:18–26
26. Evans J, Vincent CA, Bruce PG (1987) Polymer 28:2324–2328
27. Gregorio JR, Cestari M (1994) J Polym Sci BPolym Phys 32:859–870
28. Abbrent S, Plestil J, Hlavata D, Lindgren J, Tegenfeldt J, Wendsjo A (2001) Polymer 42:1407–1416
29. Martinelli A, Matic A, Jacobsson P, Börjesson L, Navarra MA, Panero S, Scrosati B (2007) J Electrochem Soc 154:G183–G187
30. Tripathy SK, JrR P, Hopfinger AJ, Banik NC, Taylor PL (1979) Macromolecules 12:656–658
31. Chen HW, Chiu CY, Chang FC (2002) J Polym Sci BPolym Phys 40:1342–1353
32. Petrowsky M, Frech R (2003) Electrochim Acta 48:2093–2097
33. Raghavan SR, Riley MW, Fedkiw PS, Khan SA (1998) Chem Mater 10:244–251
34. Grillone AM, Panero S, Retamal BA, Scrosati B (1999) J Electrochem Soc 146:27–31
35. Chandra S, Sekhon SS, Arora N (2000) Ionics 6:112–118
36. Chandra S, Sekhon SS, Srivastava R, Arora N (2002) Solid State Ionics 154–155:609–619

37. Sharma JP, Sekhon SS (2007) Solid State Ionics 178:439–445
38. Kumar D, Hashmi SA (2010) J Power Sources 195:5101–5108
39. Choi BK, Shin K (1996) Solid State Ionics 86–88:303–306
40. Hashmi SA, Upadhayaya HM, Thakur AK (2000) In: Chowdari BVR, Wang W (eds) Solid State Ionics: Materials and Devices. World Scientific, Singapore, pp 461–466
41. Pandey GP, Hashmi SA, Agrawal RC (2008) Solid State Ionics 179:543–549
42. Maier J (1994) Solid State Ionics 70–71:43–51
43. Maier J (1995) Prog Solid State Chem 23:171–263
44. Kumar B (2004) J Power Sources 135:215–231
45. Kumar B, Nellutla S, Thokchom JS, Chen C (2006) J Power Sources 160:1329–1335
46. Munichandraiah N, Sivasankar G, Scanlon LG, Marsh RA (1997) J Appl Polym Sci 65:2191–2199
47. Munichandraiah N, Scanlon LG, Marsh RA, Kumar B, Sircar AK (1995) J Appl Electrochem 25:857–863
48. Spahr ME, Novak P, Haas O, Nesper R (1995) J Power Sources 54:346–351
49. Kumar GG, Munichandraiah N (2001) J Power Sources 102:46–54